Korea-Australia Rheology Journal
Vol. 16, No. 1, March 2004 pp. 1-15

Element-free simulation of dilute polymeric flows using Brownian Configuration Fields

D. Tran-Canh and T. Tran-Cong*
Faculty of Engineering and Surveying, University of Southern Queensland, Toowoomba, QLD 4350, Australia
(Received April 16, 2003; final revision received October 22, 2003)

Abstract

The computation of viscoelastic flow using neural networks and stochastic simulation (CVFNNSS) is developed from the point of view of Eulerian CONNFFESSIT (calculation of non-Newtonian flows: finite elements and stochastic simulation techniques). The present method is based on the combination of radial basis function networks (RBFNs) and Brownian configuration fields (BCFs) where the stress is computed from an ensemble of continuous configuration fields instead of convecting discrete particles, and the velocity field is determined by solving the conservation equations for mass and momentum with a finite point method based on RBFNs. The method does not require any kind of element-type discretisation of the analysis domain. The method is verified and its capability is demonstrated with the start-up planar Couette flow, the Poiseuille flow and the lid driven cavity flow of Hookean and FENE model materials.

Keywords : Brownian dynamics, RBFN, stochastic simulation, viscoelastic flow, Brownian Configuration Fields, CONNFFESSIT, finite point method, element-free method.

1. Introduction

In recent time, several works concerned with hybrid simulations using Brownian dynamics (Laso and Oettinger, 1993; Feigl *et al.*, 1995; Laso *et al.*, 1997; Hulsen *et al.*, 1997; Oettinger *et al.*, 1997; Bonvin and Picasso, 1999; Laso *et al.*, 1999; Somasi and Khomami, 2000; Cormenzana *et al.*, 2001; Suen *et al.*, 2002, Tran-Canh and Tran-Cong, 2002; 2003) have been introduced to bypass the need for closed-form constitutive equations (CE) which are required in the conventional macroscopic approaches. The principal idea behind these schemes is to couple the continuum problem with Brownian dynamics. In the traditional CONNFFESSIT approach (Laso and Oettinger, 1993), also called Lagrangian CONNFFESSIT (Suen *et al.*, 2002), the polymer contribution to stress is calculated from the configuration of a large ensemble of dumbbells. On the other hand, the Brownian Configuration Fields (BCF) method (Hulsen *et al.*, 1997), also called Eulerian CONNFFESSIT (Suen *et al.*, 2002), uses an ensemble of configuration fields which represent the internal degrees of freedom of the polymer molecules. The BCF method avoids extra effort associated with the particle tracking process.

In the majority of the works relating to hybrid simulations, stochastic simulation techniques (SST for the calculation of the stress tensor) are coupled with element-based methods (e.g. FEM for the solution of the governing equations such as the continuity and momentum equations) in a micro-macroscopic approach. In general, as an alternative to element-based discretisation of the governing equations, various finite point methods can be used in the so called meshless approach (Kansa, 1990; Belytschko *et al.*, 1996; Duarte and Oden, 1996; Randles and Libersky, 1996; Dolbow and Belytschko, 1999; Mai-Duy and Tran-Cong, 2001; Atluri and Shen, 2002). In particular, Tran-Canh and Tran-Cong, (2002; 2003) coupled successfully the RBFN-based finite point method with SST for the numerical solution of the start-up Couette and 2-D viscoelastic fluid flows. In the macroscopic part, the discrete model is completely represented by a set of unstructured discrete collocation nodes in the analysis domain and on its boundary (i.e. there is no need to generate finite elements or define any topological connectivity, which is commonly referred to as truly meshless or mesh-free or element-free approach). In other words, the method can at least avoid the extra effort of meshing and re-meshing (if the problem requires) associated with the element type methods. However, effective volumes for stress averages (EVSA) can be flexibly generated around the collocation points to help determine the average polymer stress (Tran-Canh and Tran-Cong, 2003). The resultant element-free RBFN-SST method is Lagrangian as far as the microscopic part is concerned, and particle tracking could be inconvenient. A possible disadvantage of the present method is that the system matrix is dense and may be ill conditioned for large problems. However, this problem can be overcome with the use

*Corresponding author: trancong@usq.edu.au

of domain decomposition technique as will be reported elsewhere.

In this paper, an Eulerian element-free RBFN-SST method is developed following the Brownian Configuration Fields idea. In the present method, the polymer contribution to stress at all collocation points is calculated using the BCF technique and then the continuity and momentum equations are solved using the RBFN-based method for the velocity field and pressure. The paper is organized as follows: Sections 2 is an outline of the scheme in which the governing PDEs and SDEs for the elastic dumbbell models are briefly reviewed. In sections 3, the RBFN-based numerical method for solving the conservation equations is briefly described, followed by numerical methods of the solution of BCFs. The associated variance reduction techniques are described for the SDEs for the Hookean and FENE dumbbell models. Section 4 presents the algorithm of the present scheme for viscoelastic flow problems, highlighting the macroscopic-microscopic interfaces of the method. Numerical examples are then discussed in section 5, followed by a brief conclusion in section 6.

2. Governing equations

The present work is concerned with the flow of dilute polymer solutions which are modelled as an incompressible suspension of non-interacting macromolecules in a Newtonian solvent. Under isothermal and steady state condition, an application of the penalty function method transforms the governing equations into

$$2\eta_N \nabla \cdot \boldsymbol{L} + \rho(\boldsymbol{u}\cdot\nabla)\boldsymbol{u} + p_e \nabla(\nabla\cdot\boldsymbol{u}) = -\nabla\cdot\boldsymbol{\tau}^p, \tag{1}$$

where the penalty equation is given by

$$p = -p_e(\nabla\cdot\boldsymbol{u}), \tag{2}$$

subject to boundary conditions

$$u = u_o, \quad x \in \Gamma_u,$$
$$\boldsymbol{n}\cdot\nabla\boldsymbol{u} = q_o, \quad x \in \Gamma_t,$$

where $\boldsymbol{u}$ denotes the velocity field; $\boldsymbol{n}$ is the unit vector outwardly normal to the boundary; $\boldsymbol{L}$ is the rate of strain tensor; η_N is the Newtonian solvent viscosity; $\boldsymbol{\tau} = \boldsymbol{\tau}^s + \boldsymbol{\tau}^p = 2\eta_N\boldsymbol{L} + \boldsymbol{\tau}^p$ is the extra stress; ρ is the fluid density; p_e is a sufficiently large penalty parameter. Although this method produces an error of $O(p_e^{-1})$ (Baker, 1983) in approximating $\nabla\cdot\boldsymbol{u} = 0$, it is considered as a good method which allows the elimination of the incompressibility condition and a corresponding reduction of the number of degrees of freedom of the problem in solving complex problems (Hughes *et al.*, 1979; Crochet *et al.*, 1984; Bernstein *et al.*, 1994; Laso *et al.*, 1997; 1999). Travis *et al.* (1990) have made rigorous comparison between a number of numerical methods and concluded that the methods based on penalty function produce comparably accurate results. The value of the penalty parameter can only be chosen from experience at this stage and the value chosen in this work is based on the results reported in the references cited above.

The system is closed by the specification of a method to calculate the polymer contribution to the stress $\boldsymbol{\tau}^p$. Here, the microscopic method employs the Brownian dynamics simulation (or SST) to determine the polymer contribution to stress $\boldsymbol{\tau}^p$ via kinetic modelling (Bird *et al.*, 1987; Oettinger, 1996; Halin *et al.*, 1998). The kinetic theory-based models used here are the Hookean, FENE and FENE-P dumbbell models. These models consist of non-interacting elastic dumbbells having two Brownian beads connected by an entropic spring. The configuration of a dumbbell satisfies a certain stochastic differential equation (SDE) as detailed in Laso and Oettinger (1993) where the CONNFFESSIT idea was first proposed. In this approach, it is necessary to convect a large number of molecules through the domain under consideration, hence there are some extra effort associated with particle tracking (Hulsen *et al.*, 1997; Laso, 1998).

Hulsen *et al.* (1997) proposed a modified CONNFFESSIT method which overcomes these drawbacks. The method employs an ensemble of N continuous configuration fields $\boldsymbol{Q}(\boldsymbol{x},t)$ with respect to space and time instead of convecting discrete connector vectors $\boldsymbol{Q}_i$'s. The main idea of this scheme is that after initiating N spatially uniform configuration fields $(N,\boldsymbol{Q})$ whose values are independently sampled from an equilibrium distribution function, the configuration fields are convected and deformed by the drift component (flow gradient, elastic retraction) and by the diffusion component (Brownian motion). This evolution of a configuration field satisfies the following SDE

$$d\boldsymbol{Q}(t) = \left[-\boldsymbol{u}\cdot\nabla\boldsymbol{Q} + \boldsymbol{\kappa}\cdot\boldsymbol{Q} - \frac{2}{\zeta}\boldsymbol{F}(\boldsymbol{Q})\right]dt + \sqrt{\frac{4k_BT}{\zeta}}\,d\boldsymbol{W}(t), \tag{3}$$

where ζ is the friction coefficient between the dumbbell and the solvent; k_B is Boltzmann constant; T is the absolute temperature; $\boldsymbol{W}(t)$ is a 3-component vector which is a Wiener process with mean $\langle \boldsymbol{W}_i(t)\rangle = 0$ and covariance $\langle \boldsymbol{W}_i(t)\boldsymbol{W}_j(t')\rangle = \delta_{ij}\min(t,t')$ and accounts for the random displacement of the beads due to thermal motion; $\boldsymbol{\kappa} = (\nabla\boldsymbol{u})^T$ is the velocity gradient; $\boldsymbol{F}$ is the spring connector force between the two beads and depends on the model. Letting H be the spring constant, the connector force is given by

$$\boldsymbol{F} = H\boldsymbol{Q}, \tag{4}$$

$$\boldsymbol{F} = H\frac{\boldsymbol{Q}}{1-\left(\frac{\boldsymbol{Q}}{Q_o}\right)^2}, \tag{5}$$

for the Hookean and the FENE dumbbell models, respectively, where Q_o is the maximum possible spring length. The configuration fields $(N,\boldsymbol{Q})$ are obtained by solving the

SDE eqn. (3). The term $\boldsymbol{u}(\boldsymbol{x},t)\cdot\nabla\boldsymbol{Q}(\boldsymbol{x},t)$ accounts for the convection of the configuration fields by the flow. Since $d\boldsymbol{W}$ depends on time only, it affects the configuration fields in a spatially uniform way and hence the gradient of the configuration fields is well defined as smooth functions of the spatial coordinates (Hulsen *et al.*, 1997). It can be seen that the existence of the convective term in this Eulerian framework is completely equivalent to the particle tracking in the traditional Lagrangian CONNFFESSIT approach. Once the configuration fields are known, the stress can be determined as follows

$$\boldsymbol{\tau}^p = -n_d k_B T\boldsymbol{I} + n_d\langle\boldsymbol{Q}\cdot\boldsymbol{F}\rangle, \tag{6}$$

where n_d is the density of dumbbells; $\boldsymbol{I}$ is the identity tensor and $\boldsymbol{F}$ is the spring force. The configuration field $\boldsymbol{Q}$ is non-dimensionalised by $\sqrt{k_BT/H}$, and equation (3) becomes

$$d\boldsymbol{Q}' = \left[-\boldsymbol{u}(x,t)\cdot\nabla\boldsymbol{Q}'(x,t) + \boldsymbol{\kappa}(x,t)\cdot\boldsymbol{Q}'(x,t) - \frac{1}{2\lambda_H}\boldsymbol{F}'(\boldsymbol{Q}')\right]dt + \sqrt{\frac{1}{\lambda_H}}d\boldsymbol{W}(t), \tag{7}$$

where $\boldsymbol{Q}' = \boldsymbol{Q}[H/(k_BT)]^{1/2}$ is the dimensionless form of the configuration field vector $\boldsymbol{Q}$; $\lambda_H = \zeta/(4H)$ is the relaxation time of dumbbells; $b = \frac{HQ_0^2}{k_BT}$ is the square of the maximum possible extension of the dimensionless configuration field $\boldsymbol{Q}'$ and $\boldsymbol{F}'$ is the dimensionless spring force given by

$$\boldsymbol{F}' = \boldsymbol{Q}', \tag{8}$$

$$\boldsymbol{F}' = \frac{\boldsymbol{Q}'}{1-\frac{\boldsymbol{Q}'^2}{b}} \tag{9}$$

for the Hookean and FENE dumbbell models, respectively. For the sake of brevity, primes will be dropped in the following discussion.

3. Computational schemes

In this section, computational techniques are described for the numerical solution of the conservation equations (momentum and continuity equations) and the Brownian configuration fields, respectively. For the stochastic processes, a variance reduction technique is described, followed by a presentation of the overall algorithm.

3.1. RBFN-based element-free method for solving the momentum and continuity equations

An element-free method based on RBFNs for solving PDEs was developed and reported elsewhere (e.g. Tran-Canh and Tran-Cong, 2003). Briefly, the method takes advantage of the fact that a smooth function can be approximated by a RBFN such as (Haykin, 1999; Golberg *et al.*, 1996)

$$f(\boldsymbol{x}) = \sum_{j=1}^{m} w^j h^j\boldsymbol{x} + \sum_{k=1}^{\bar{m}} \boldsymbol{\lambda}^k p^k(\boldsymbol{x}) = \boldsymbol{R}^T(\boldsymbol{x})\boldsymbol{w} + \boldsymbol{P}^T(\boldsymbol{x})\boldsymbol{\lambda} \tag{10}$$

$$\sum_{i=1}^{m} p^k(\boldsymbol{x}_i)w^i = 0, \quad k = 1,.....,\bar{m} \tag{11}$$

where $w^j \in \boldsymbol{w}$ ($\boldsymbol{w}^T = [w^1\ w^2 ...\ w^m]$) and $\lambda^k \in \lambda$($\lambda^T = [\lambda^1\lambda^2...\lambda^{\bar{m}}]$) are the synaptic weights; h^j is the chosen radial basis function corresponding to the j^{th} RBF-neuron; p^k is the polynomial basis function corresponding to the k^{th} PBF-neuron; $m + \bar{m}$ is the total number of neurons. $\boldsymbol{R}$ and $\boldsymbol{P}$ are defined as follows

$$R^T(x) = [h^1(x)h^2(x)...h^m(x)], \tag{12}$$

$$P^T(x) = [p^1(x)p^2(x)...p^{\bar{m}}(x)]. \tag{13}$$

Let n be the number of collocation points $(\boldsymbol{x}_i, \hat{y}_i)$; $\boldsymbol{x}_i$ is the coordinate of the i^{th} collocation point and $\hat{y}_i$ is the desired value of function f at the collocation point $\boldsymbol{x}_i$. The RBF h^j employed here is the Thin Plate Splines (TPS-RBF) (Duchon, 1976) which is given by

$$h^j(\boldsymbol{r}) = h^j(\|\boldsymbol{x}-\boldsymbol{c}^j\|) = r^{2s}\log(r), \quad s = 1,2,..., \tag{14}$$

of which the corresponding first and second order derivatives are given respectively by

$$\frac{\partial h^j}{\partial x^j} = r^{2(s-1)}(x_i - c_i^j)(2s\log(r)+1) \tag{15}$$

$$\frac{\partial^2 h^j}{\partial x_i \partial x_l} = 2r^{2(s-2)}(x_i - c_i^j)(x_1 - x_l^j)[2s(s-1)\log(r) + (2s-1)] + \chi(r),$$

$$\chi(r) = r^{2(s-1)}(2s\log(r)+1) \quad \forall i = 1,$$

$$\chi(r) = 0 \quad \forall i \neq 1 \tag{16}$$

where $\boldsymbol{r} = \boldsymbol{x} - \boldsymbol{c}^j$ and $r = \|\boldsymbol{x} - \boldsymbol{c}^j\|$ is the Euclidean norm of $\boldsymbol{r}$; $\{\boldsymbol{c}\}^m{}_{j=1}$, with $m \le n$, is a set of RBF centers that can be chosen from among the training points; $a^j > 0$ is the width of the j^{th} RBF (Haykin, 1999). Since the TPS-RBF is C^{2s-1}-continuous, the power index s must be appropriately chosen for a given partial differential operator (Zerroukat *et al.*, 1998). In the present work, the TPS-RBF with $s = 2$ is chosen to satisfy the continuity condition. For 2D problems, the first order PBF is used as follows

$$P^T(x) = [1\ \ x_1\ \ x_2]. \tag{17}$$

It is interesting to note that the TPS-RBF does not contain any adjustable parameter and in some situations the TPS-RBFN methods can achieve an accuracy similar to that of the Multi-Quadric RBFN (MQ-RBFN) (Zerroukat *et al.*, 1998; 2000; Tran-Canh and Tran-Cong, 2002).

3.1.1. RBF-centres, collocation points and RBFN training

The choice of the quantity and location of collocation points ($\boldsymbol{x}_i$, $i = 1,...,n$) depends on the problem geometry and desired solution accuracy and is a major open issue requir-

ing separate investigation (Fodoseyev *et al.*, 2000; Orr, 1999; Larsson and Fornberg, 2001). However, one can imagine an analogy between an adaptive discretisation in the present finite point method and a finite element method. In this respect, an advantage of the present finite point method is that points can be added or removed much more easily than a corresponding addition or removal of finite elements, since there is no topology to be concerned about. In general, both collocation points and RBF centres can be randomly and separately distributed in the analysis domain. However, in the present work, collocation points are chosen to be the same as RBF centres, i.e. m = n, which are uniformly distributed in the physical domain. The unknown weights are found by minimizing an appropriate cost function given by

$$\boldsymbol{C}(w,\Lambda)=\sum_{i=1}^{n}(\hat{y}_i-f(x_i))^2+\Lambda\sum_{j=1}^{m}W^{(j)2}, \tag{18}$$

where Λ is a global regularization parameter; $w\in \boldsymbol{w}'$, $(\boldsymbol{w}'^T=[w^1,w^2,...,w^m])^j$.

Then the partial derivatives of $f(\boldsymbol{x})$ can be calculated analytically as follows

$$\mathcal{L}f(\boldsymbol{x})=\sum_{j=1}^{m}w^j\mathcal{L}h^j(x)+\sum_{k=1}^{\bar{m}}\lambda^k\mathcal{L}p^k(x), \tag{19}$$

where Λ is a derivative operator.

In particular, each variable in the momentum and continuity equations is approximated by an RBFN such as (10), and those equations are collocated at chosen points throughout the analysis domain, yielding the following sum square error without penalty method (planar flows in dimensionless form)

$$\begin{aligned}SSE=&\sum\left\{\frac{\partial u_1}{\partial x_1}+\frac{\partial u_2}{\partial x_2}\right\}_i^2\\&+\sum\left\{\alpha\left[\frac{\partial^2 u_1}{\partial x_1^2}+\frac{\partial^2 u_1}{\partial x_2^2}\right]-Re\left[u_1\frac{\partial u_1}{\partial x_1}+u_2\frac{\partial u_1}{\partial x_2}\right]-\frac{\partial p}{\partial x_1}+\left[\frac{\partial \tau_{11}^p}{\partial x_1}+\frac{\partial \tau_{21}^p}{\partial x_2}\right]\right\}_i^2\\&+\sum\left\{\alpha\left[\frac{\partial^2 u_2}{\partial x_1^2}+\frac{\partial^2 u_2}{\partial x_2^2}\right]-Re\left[u_1\frac{\partial u_2}{\partial x_1}+u_2\frac{\partial u_2}{\partial x_2}\right]-\frac{\partial p}{\partial x_2}+\left[\frac{\partial \tau_{12}^p}{\partial x_1}+\frac{\partial \tau_{22}^p}{\partial x_2}\right]\right\}_i^2\\&+\sum_{i\in\Gamma_u}\{u_1-u_o\}^2+\sum_{i\in\Gamma_t}\left\{\left[n_1\frac{\partial u_1}{\partial x_1}+n_2\frac{\partial u_1}{\partial x_2}\right]-q_o\right\}_i^2\end{aligned} \tag{20}$$

and with penalty method

$$\begin{aligned}SSE=&\sum\left\{\alpha\left[\frac{\partial^2 u_1}{\partial x_1^2}+\frac{\partial^2 u_1}{\partial x_2^2}\right]-Re\left[u_1\frac{\partial u_1}{\partial x_1}+u_2\frac{\partial u_1}{\partial x_2}\right]+p_e\left[\frac{\partial^2 u_1}{\partial x_1^2}+\frac{\partial^2 u_1}{\partial x_1\partial x_2}\right]+\Phi_{1i}\right\}_i^2\\&+\sum\left\{\alpha\left[\frac{\partial^2 u_2}{\partial x_1^2}+\frac{\partial^2 u_2}{\partial x_2^2}\right]-Re\left[u_1\frac{\partial u_2}{\partial x_1}+u_2\frac{\partial u_2}{\partial x_2}\right]+p_e\left[\frac{\partial^2 u_2}{\partial x_2^2}+\frac{\partial^2 u_1}{\partial x_1\partial x_2}\right]+\Phi_{2i}\right\}_i^2\\&+\sum_{i\in\Gamma_u}\{u_1-u_o\}^2+\sum_{i\in\Gamma_t}\left\{\left[n_1\frac{\partial u_1}{\partial x_1}+n_2\frac{\partial u_2}{\partial x_2}\right]-q_o\right\}_i^2\end{aligned} \tag{21}$$

where i denotes the i^{th} collocation point; $\alpha=\eta_N/\eta_o$; $\eta_o=\eta_N+\eta_p$; η_p is the polymer viscosity; $Re=\rho Va/\eta_o$, V and a are characteristic velocity and length, respectively; $\Phi_{1i}=\frac{\partial \tau_{11}^p}{\partial x_1}(x_i)+\frac{\partial \tau_{21}^p}{\partial x_2}(x_i)$; $\Phi_{2i}=\frac{\partial \tau_{12}^p}{\partial x_1}(x_i)+\frac{\partial \tau_{22}^p}{\partial x_2}(x_i)$. The stresses are scaled by $\eta_o V/a$. Applying the general linear least square principle to (20) or (21) (taking into account (11)), a system of linear algebraic equations of the unknown weights is obtained as follows

$$(\boldsymbol{B}^T\boldsymbol{B})\boldsymbol{w}'=\boldsymbol{B}^T\hat{\boldsymbol{y}} \tag{22}$$

where $\boldsymbol{B}$ is the design matrix; $\boldsymbol{w}'$ is the vector of all weights; $\hat{\boldsymbol{y}}$ is the vector of known values. The non-linear convective term $(\boldsymbol{u}\cdot\nabla)\boldsymbol{u}$ in (20)-(21) is estimated using a Picard-type iterative procedure whose detail can be found in Tran-Canh and Tran-Cong (2003).

3.2. Numerical solution of the configuration fields

In the present work, two numerical schemes are used to solve the SDE, namely the explicit Euler and the semi-implicit predictor-corrector scheme. The former is relative simple and therefore not detailed here. The latter for the time discretisation of the elastic dumbbell configuration fields was described in Gardiner (1990) Oettinger (1996) Kloeden and Platen, (1995) and Somasi *et al.* (2000) and therefore is presented only briefly for the FENE model. The technique consists of two steps as follows

(a) The predictor step

Let $\boldsymbol{Q}_i=\boldsymbol{Q}(t_i)$, using a fixed time stepsize Δt for the stochastic process, the predicted BCF $\boldsymbol{Q}^*_{n+1}$ at the time step t_{n+1} is explicitly determined as follows:

$$\boldsymbol{Q}^*_{(n+1)}=\boldsymbol{Q}_n-\left(\boldsymbol{u}_n\cdot\nabla\boldsymbol{Q}_n-\boldsymbol{\kappa}_n\cdot\boldsymbol{Q}_n+\frac{\boldsymbol{Q}_n}{2\lambda_H\left(1-\frac{\boldsymbol{Q}_n^2}{Q_o}\right)}\right)\Delta t+\sqrt{\frac{\Delta t}{\lambda_H}}W_n, \tag{23}$$

The updated configuration fields $\boldsymbol{Q}^*_{n+1}$'s are employed to estimate the polymer contribution to the predicted stress $\boldsymbol{\tau}^*_{n+1}$, according to (6), which is in turn used to get the solutions of the predicted velocity at time t_{n+1} by solving eqn. (1).

(b) The corrector step

$$\left(1+\frac{\Delta t}{4\lambda_H\left(1-\frac{\boldsymbol{Q}^2_{n+1}}{b}\right)}\right)\boldsymbol{Q}_{(n+1)}=\boldsymbol{Q}_n+\frac{1}{2}\Big(-\boldsymbol{u}_n\cdot\nabla\boldsymbol{Q}_n-\boldsymbol{u}^*_{n+1}\cdot\nabla\boldsymbol{Q}^*_{n+1}$$

$$+\boldsymbol{\kappa}_n\cdot\boldsymbol{Q}_n+\boldsymbol{\kappa}^*_{n+1}\cdot\boldsymbol{Q}^*_{n+1}-\frac{\boldsymbol{Q}_n}{2\lambda_H\left(1-\frac{\boldsymbol{Q}_n^2}{Q_o}\right)}\Bigg)+\sqrt{\frac{\Delta t}{\lambda_H}}\boldsymbol{W}_n \tag{24}$$

Eqn. (24) leads to a unique cubic equation for $|\boldsymbol{Q}_{n+1}|$ of which admissible solutions are those that satisfy $0 \le |\boldsymbol{Q}_{i+1}| < \sqrt{b}$ (Oettinger, 1996). It is noted that in the present work, the gradients of the configuration and velocity on the RHS of (23)-(24) are determined by calculating directly the derivatives of their TPS-RBFN approximant as shown in eqn. (19).

The polymer stress tensor is then determined by the average of the configuration fields evaluated at each collocation point and given by Kramers' expression as follows (Bird *et al.*, 1987; Oettinger, 1996):

$$\boldsymbol{\tau}=-n_d k_B T(\langle\boldsymbol{QQ}\rangle-\boldsymbol{I}) \tag{25}$$

$$\boldsymbol{\tau}=-n_d k_B T\left(\frac{\langle\boldsymbol{QQ}\rangle}{1-\frac{\boldsymbol{Q}^2}{b}}-\boldsymbol{I}\right) \tag{26}$$

for the Hookean and FENE dumbbell models, respectively.

3.3. Variance reduction method

Without increasing the number of dumbbells, in polymer dynamics, a method is available to reduce the variance, but not to change the average value of the parameters of interest (Melchior and Oettinger, 1996; Oettinger *et al.*, 1997; Bonvin and Picasso, 1999). The variance reduction consists of different techniques which are detailed in Oettinger *et al.* (1996); Kloeden and Platen (1995) and Kloeden *et al.* (1997). Owing to the Eulerian nature of the BCF scheme, the implementation of the variance reduction techniques is achieved easily in the present approach. In this work, the control variate method is presented only for the FENE dumbbell model. Discussions on the efficiency of the scheme can be found in those references cited earlier (Melchior and Oettinger, 1996; Oettinger *et al.*, 1997; Bonvin and Picasso, 1999) and are not repeated here.

3.3.1. Control variate method for the FENE dumbbell model

The method uses a control variate $\boldsymbol{X}_c$ which is correlated with a random variable $\boldsymbol{X}$, to produce a better estimator of $\langle\boldsymbol{X}\rangle$. While $\langle\boldsymbol{X}\rangle$ is unknown and needs to be estimated, $\langle\boldsymbol{X}_c\rangle$ can be calculated by a deterministic method. The method has been applied in other studies more recently (Jendrejack *et al.*, 2000; Kroger *et al.*, 2000 and Prabhakar and Prakash, 2002). In the Brownian Configuration Fields method, the control variate reduction technique is implemented as follows: at each collocation point, N dumbbells are assigned and numbered from $i = 1 .. N$ where dumbbells having the same index in the whole analysis domain have the same random number. Here, for illustrative purpose, this technique is presented for the numerical calculation of the polymer contribution to stress using the FENE model (26) where the expectation of random variable $\frac{\boldsymbol{QQ}}{1-\boldsymbol{Q}^2/b}$ is required. At each time t and position $\boldsymbol{x}$, let $\bar{\boldsymbol{Q}}(\boldsymbol{x}, t)$ be the control variate corresponding to the configuration field $\boldsymbol{Q}(\boldsymbol{x}, t)$. The variance reduction method is carried out by splitting the expectation above as follows (Bonvin and Picasso, 1999)

$$\left\langle\frac{\boldsymbol{QQ}}{1-\frac{\boldsymbol{Q}^2}{b}}\right\rangle=\left\langle\frac{\bar{\boldsymbol{Q}}\,\bar{\boldsymbol{Q}}}{1-\frac{\bar{\boldsymbol{Q}}^2}{b}}\right\rangle+\left\langle\frac{\boldsymbol{QQ}}{1-\frac{\boldsymbol{Q}^2}{b}}-\frac{\bar{\boldsymbol{Q}}\,\bar{\boldsymbol{Q}}}{1-\frac{\bar{\boldsymbol{Q}}^2}{b}}\right\rangle. \tag{27}$$

When $\bar{\boldsymbol{Q}}=0$ there is no variance reduction. From (27), the polymer stress tensor (26) is rewritten as follows

$$\boldsymbol{\tau}^p=n_d k_B T\left\langle\frac{\boldsymbol{QQ}}{1-\frac{\boldsymbol{Q}^2}{b}}-\frac{\bar{\boldsymbol{Q}}\,\bar{\boldsymbol{Q}}}{1-\frac{\bar{\boldsymbol{Q}}^2}{b}}\right\rangle+\bar{\boldsymbol{\tau}}^p_{fene}, \tag{28}$$

where

$$\bar{\boldsymbol{\tau}}^p_{fene}=-n_d k_B T\left(\left\langle\frac{\bar{\boldsymbol{Q}}\,\bar{\boldsymbol{Q}}}{1-\frac{\bar{\boldsymbol{Q}}^2}{b}}\right\rangle-\boldsymbol{I}\right). \tag{29}$$

The first term of the RHS of (28) is calculated by using Brownian dynamics simulations and the second term is determined in a deterministic way. In the present work, since $\bar{\boldsymbol{Q}}$'s are estimated at equilibrium configuration $\boldsymbol{\tau}^p{}_{fene}$ is zero and the configuration vectors $\bar{\boldsymbol{Q}}$'s satisfy the following SDE

$$d\bar{\boldsymbol{Q}}=-\frac{\bar{\boldsymbol{F}}}{2\lambda_H}dt+\sqrt{\frac{1}{\lambda_H}}d\boldsymbol{W}(t), \tag{30}$$

where $\bar{F}$ is determined by (9). The polymer stress tensor (28) reduces to

$$\boldsymbol{\tau}^p=-n_d k_B T\left\langle\frac{\boldsymbol{QQ}}{1-\frac{\boldsymbol{Q}^2}{b}}-\frac{\bar{\boldsymbol{Q}}\,\bar{\boldsymbol{Q}}}{1-\frac{\bar{\boldsymbol{Q}}^2}{b}}\right\rangle. \tag{31}$$

4. Algorithm of the present method

In general, the overall approach can now be described in a detailed algorithm (see Figs. 1 and 2 for flowcharts) as follows:

a. Generate a set of collocation points and start with an initial velocity for the first iteration (zero in the present work) along with the boundary conditions of problem;

b. Assign N dumbbells to each collocation point. These dumbbells are numbered from $i = 1$ to N. All dumbbells having the same index constitute a configuration. Hence there is an ensemble of N configuration fields $\boldsymbol{Q}_i$ ($i = 1 .. N$). Initially, the polymer configuration fields are spatially uniform and their values are independently sampled from the known equilibrium distribution function which is a 3-

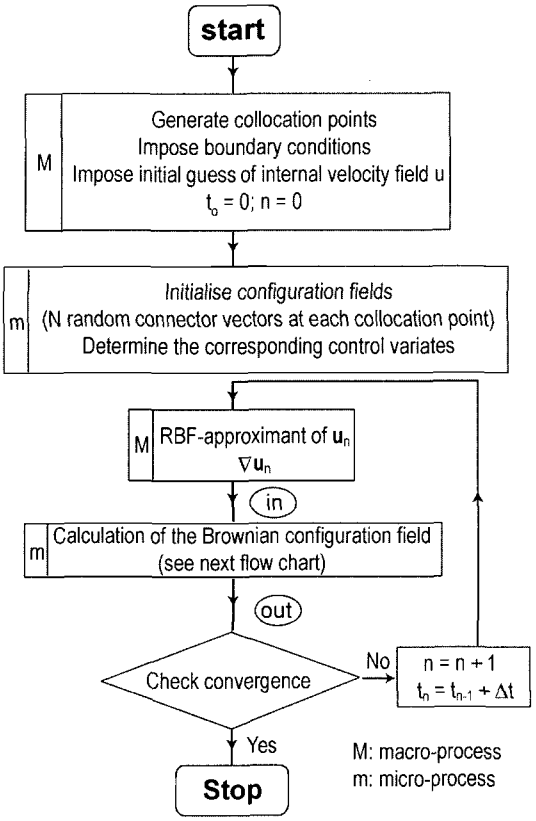

Fig. 1. General flow-chart of the present element-free RBFN-SST method. See Fig. 2 for details of the calculation of the BCF.

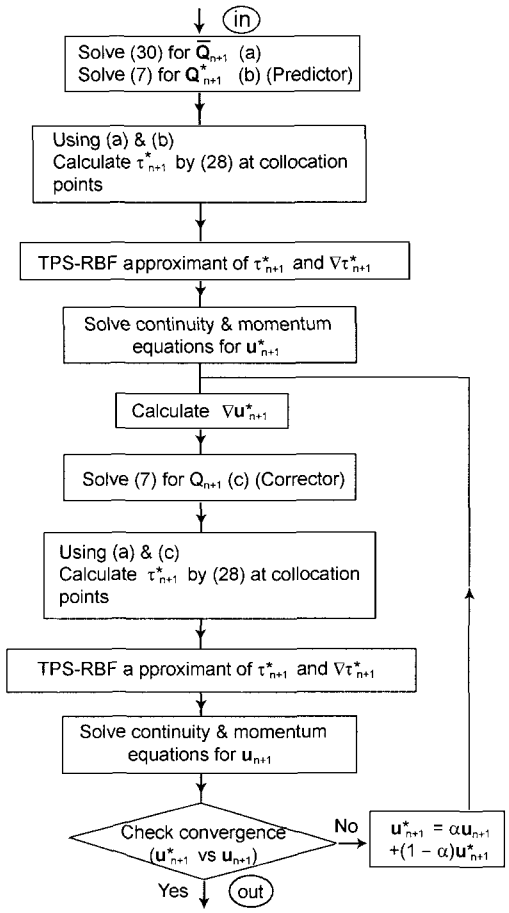

Fig. 2. Details of the calculation of the BCF using semi implicit predictor corrector method. This flowchart represents part of the overall flowchart shown in Fig. 1.

D Gaussian distribution with zero mean and unit covariance (Bird *et al.*, 1987; Oettinger, 1996). Since all the dumbbells having the same index receive the same random numbers, there is a strong correlation between dumbbells in a configuration. The control variates $\bar{\boldsymbol{Q}}$'s associated with the configuration fields $\boldsymbol{Q}_i$'s are created as described in section 3.3;

c. Calculate velocity gradient fields directly by differentiating the RBFNs that approximate the velocity fields;

d. Calculate the polymer configuration fields using the method described in section 3.2. To ensure strong correlation within a configuration field, all the dumbbells of the same index have the same random numbers. For each configuration field $\boldsymbol{Q}$, a corresponding control variate $\bar{\boldsymbol{Q}}$ is determined according to the procedure described in section 3.3. In this work, while the time discretisation of the BCF is carried out by a predictor-corrector scheme, the control variates which are governed by eqn. (30) is estimated by Euler method;

e. Determine the polymer contribution to stress by taking the ensemble average of the polymer configurations at each collocation point, using (28) for the FENE dumbbell model for example. Impose the stress boundary conditions at the collocation points located on the boundary;

f. The stress is then approximated globally by TPS-RBF networks which are the ultimate description of the stress field;

g. With the stress field just obtained, solve the set of conservation equations for the new velocity field using the RBFN-based mesh-free method as described in sections 3.1;

h. Terminate the simulation when either the desired time or convergence is reached. The latter is determined by a convergence measure for either the velocity field or the stress field, which is defined for the velocity field by

$$CM = \sqrt{\frac{\sum_{1}^{N}\sum_{i=1}^{d}(u_i^n - u_i^{n-1})^2}{\sum_{1}^{N}\sum_{i=1}^{d}(u_i^n)^2}} < tol \tag{32}$$

where d is the number of dimension (2 in the present work); tol is a preset tolerance; u_i is the i component of the velocity at a collocation point; N is the total number of col-

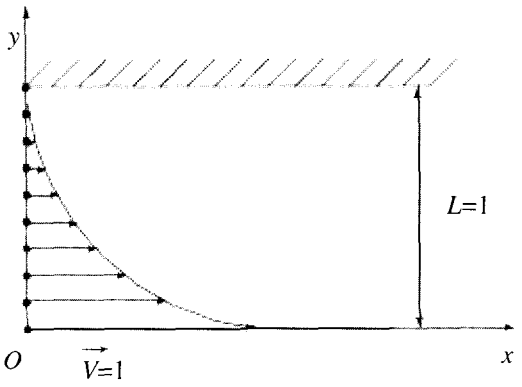

Fig. 3. The start-up planar Couette flow problem: the bottom plate moves with a constant velocity $V = 1$, the top plate is fixed; no-slip boundary conditions apply at the fluid-solid interfaces. The collocation point distribution is only schematic.

location points and n is the iteration number. Convergence is also checked for the shear stress and the first normal stress difference;

i. Return to step (d) for the next time level of the microscopic process.

5. Numerical examples

The present method is verified with the simulation of the start-up planar Couette and steady state planar Poiseuille flows of Hookean and FENE model fluids. The capability of the method is then demonstrated with the simulation of the lid driven cavity flow of the Hookean model fluid. For all examples, the criterion for convergence is $tol = 10^{-4}$ applied to the velocity field.

5.1. Start-up planar Couette flow

This problem was earlier studied by Mochimaru (1983) for the FENE-P model, by Laso and Oettinger (1993) and Tran-Canh and Tran-Cong (2002) for the FENE and FENE-P models, and it is used here to verify the present method. The problem is defined in Fig. 3. and the chosen physical parameters are $\eta_o = \eta_N + \eta_p = 1$, $\rho = 1.2757$, $\lambda_H = 49.62$, $b = 50$, $\eta_N = 0.0521$, $\Delta t = 10^{-2}$ (Mochimaru, 1983; Laso and Oettinger, 1993).

To ensure that the centre density is adequate, three levels of discretisation are used, namely $n = 17$, $n = 23$ and $n = 25$, and the results show that the solutions obtained do not differ significantly. Only the results corresponding to $n = 25$ are presented here. The analysis is carried out for the FENE dumbbell model where the configuration fields are produced with one thousand dumbbells at each collocation point and the velocity convergence is shown in Fig. 4. The control variate is calculated at the equilibrium state. The simulation is continued for $t \geq 0$ until the flow reaches the steady state.

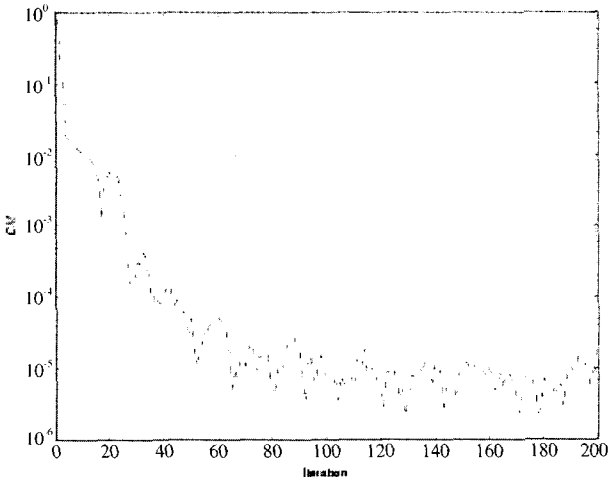

Fig. 4. The steady-state planar Couette flow problem using the FENE model: the velocity convergence rate. The parameters of the problem are number of collocation points = 25, the number of dumbbells at each collocation point = 1000, $\lambda_H = 49.62$, $b = 50$, $\eta_N = 0.0521$ and $\Delta t = 10^{-2}$.

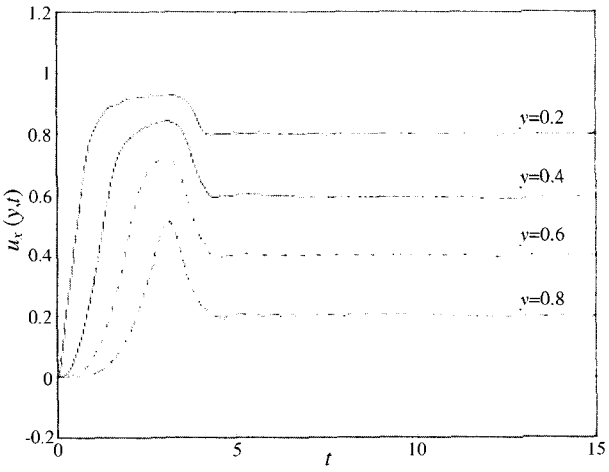

Fig. 5. The steady-state planar Couette flow problem using the FENE model: the time evolution of velocity at locations $y = 0.2$, $y = 0.4$, $y = 0.6$ and $y = 0.8$. The parameters of the problem are number of collocation points = 25, the number of dumbbells at each collocation point = 1000, $\lambda_H = 49.62$, $b = 50$, $\eta_N = 0.0521$ and $\Delta t = 10^{-2}$.

Fig. 5 describes the evolution of the velocity at four locations $y = 0.2$, $y = 0.4$, $y = 0.6$ and $y = 0.8$ and shows that the velocity overshoot occurs sooner in fluid layers nearer to the moving wall. Fig. 6 depicts the evolution of the velocity profile with respect to the coordinate y, which confirms that velocity undershoot is insignificant in comparison with overshoot. Figs. 7 and 8 describe the evolution of the shear stress and the first normal stress difference, respectively at locations $y = 0.2$, $y = 0.4$, $y = 0.6$ and $y = 0.8$. The present result is a close match with the results of CONNFFESSIT (Laso and Oettinger, 1993) and CVFNNSS (Tran-Canh

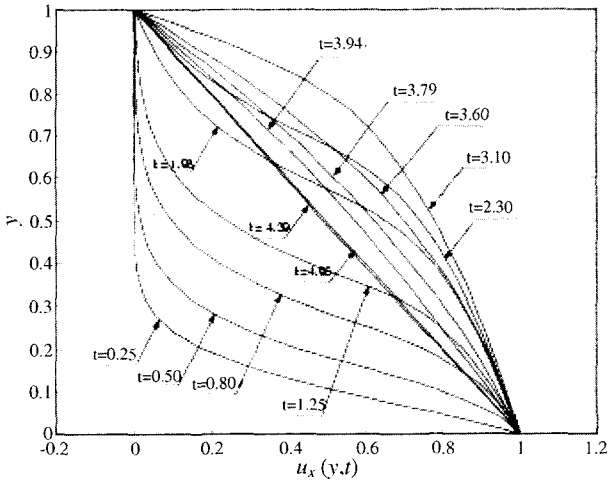

Fig. 6. The steady-state Couette flow problem using the FENE dumbbell model: the velocity profile with respect to location y at different times. The parameters are the same as in Fig. 5.

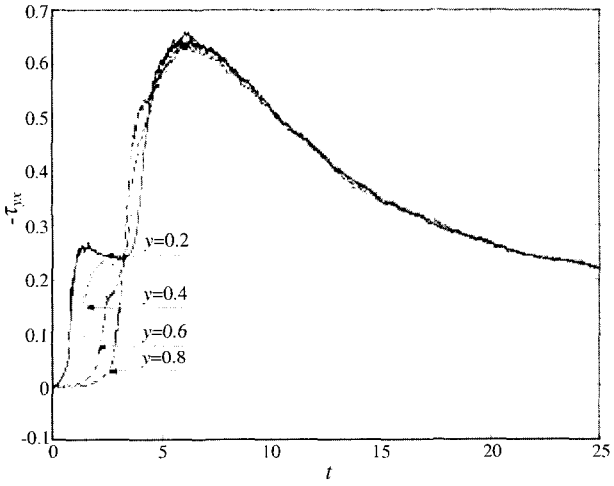

Fig. 7. The steady-state planar Couette flow problem using the FENE dumbbell model: the evolution of shear stress at location $y = 0.2$, $y = 0.4$, $y = 0.6$, $y = 0.8$ with respect to time. The parameters are the same as shown in Fig. 5.

and Tran-Cong, 2002). It is notable that the quality of convergence is better than that achieved with the CVFNNSS method.

5.2. The steady state planar Poiseuille flow

The planar creeping Poiseuille problem and coordinate system are described in Fig. 9a where only half of the fluid domain needs to be considered, owing to symmetry. For this problem, the characteristic length is chosen to be a, half of the gap between the two parallel plates; the characteristic velocity V, the maximum velocity; the characteristic viscosity $\eta_o = \eta_N + \eta_p$; and the characteristic time λ_H. The length of the domain under consideration is a.

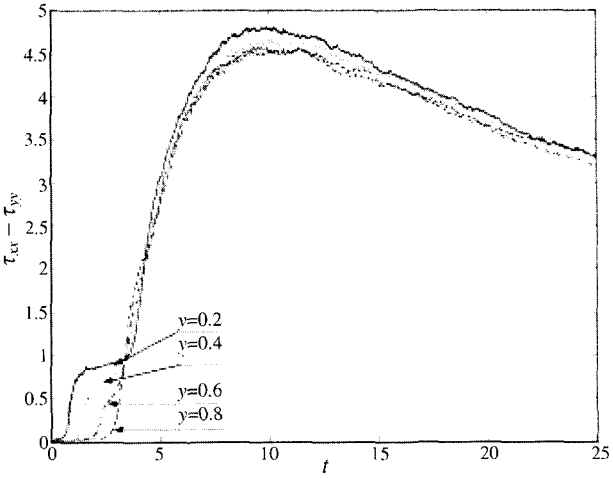

Fig. 8. The steady-state planar Couette flow problem using the FENE dumbbell model: the evolution of the first normal stress difference at location $y = 0.2$, $y = 0.4$, $y = 0.6$, $y = 0.8$ with respect to time. The parameters are the same as shown in Fig. 5.

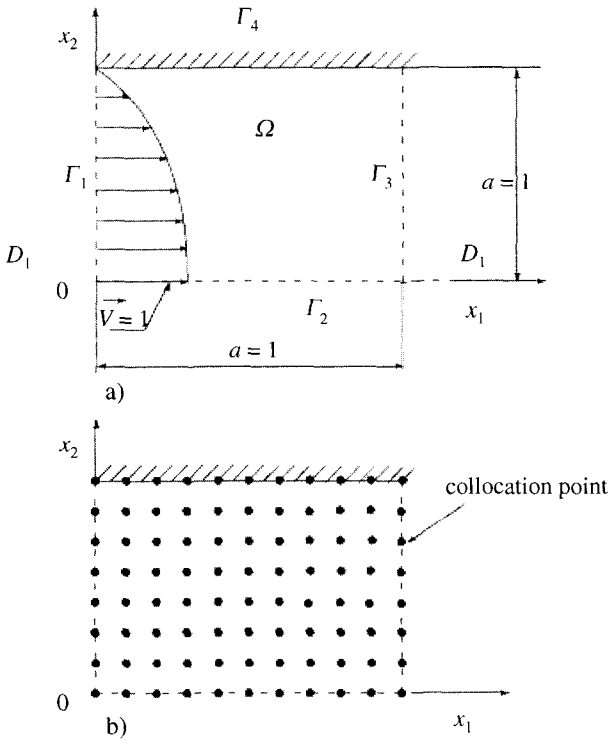

Fig. 9. a) The planar Poiseuille flow problem with parabolic inlet velocity profile; non-slip boundary conditions applied at the fluid-solid interfaces. b) The collocation point distribution is only schematic.

Using two collocation densities, namely 15×15 and 25×25, whose schematic distribution is shown in Fig. 9b, 1000 dumbbells are assigned at each collocation point. In this example, tow models, namely Hookean and FENE, are

considered. The fluid parameters are as follows (Feigl *et al.*, 1995)

$\eta_N = 0.5;\ \eta_N/\eta_o = 0.5;\ \lambda_H = 1;\ b = 50.$

5.2.1. Boundary conditions and analytical solution

The macroscopic boundary conditions are given in dimensionless form as follows:

• On the wall (Γ_4), there is no slip

$\boldsymbol{u}(\boldsymbol{x}) = 0$

• At the inlet section (Γ_1), the flow is fully developed Poiseuille where the velocity profile is parabolic for the Hookean model as follows

$$\begin{cases} u_1(\boldsymbol{x}) = u_p = (1 - x_2^2), \\ u_2(\boldsymbol{x}) = 0. \end{cases}$$

For the FENE model, this velocity profile is not parabolic and determined by using the periodic boundary condition at the inlet and outlet. Although the planar Poiseuille flow can be computed as a 1D-problem, the 2-D method using the model FENE is carried out as follows

– Initially, the inlet of the domain is given a parabolic profile as described above for the Hookean model;

– The obtained outlet velocity profile at a step i is used to update the inlet velocity profile of the next step ($i + 1$);

– The process is continued until there is no further change in the outlet profile.

• At the outlet section ((Γ_3)

$u_2(\boldsymbol{x}) = 0,$

• On the centreline (Γ_2), the symmetry condition applies

$u_2(\boldsymbol{x}),\ \dfrac{\partial u_1}{\partial x_2}(\boldsymbol{x}),\ \tau_{12} = 0.$

For the Hookean dumbbell (Oldroyd-B) model, the creeping Poiseuille flow problem has the analytical solution given by

$$\tau_{11} = 3(1-\alpha)De\left(\frac{\partial u_1}{\partial x_2}\right)^2;\ \tau_{12} = (1-\alpha)\frac{\partial u_1}{\partial x_2};\ \tau_{22} = 0, \qquad (34)$$

where $De = \lambda_H \langle u_1 \rangle / a = 2/3\ \lambda_H V/a$ is the Deborah number and stresses are scaled by $\eta_o V/a$. The above analytical solution is used to judge the quality of the following numerical simulation.

5.2.2. Sum square error

The expression of sum square error (20) for the creeping planar Poiseuille flows is given by

$$SSE = \sum_{x_i \in \Omega} \left\{ \frac{\partial u_1}{\partial x_1}(x_i) + \frac{\partial u_2}{\partial x_2}(xi) \right\}_i^2$$

$$+ \sum \left\{ \alpha \left[\frac{\partial^2 u_1}{\partial x_1^2}(x_i) + \frac{\partial^2 u_1}{\partial x_2^2}(x_i) \right] - \frac{\partial p}{\partial x_1}(x_i) + \Phi_1(x_i) \right\}_i^2$$

$$+ \sum \left\{ \alpha \left[\frac{\partial^2 u_2}{\partial x_1^2}(x_i) + \frac{\partial^2 u_2}{\partial x_2^2}(xi) \right] - \frac{\partial p}{\partial x_2}(x_i) + \Phi_2(x_i) \right\}_i^2$$

$$\sum_{x_i \in \Gamma_1} \{u_1(x_i) - u_p\}^2 + \sum_{x_i \in \Gamma_1} u_2^2(x_i) + \sum_{x_i \in \Gamma_2} u_2^2(x_i) + \sum_{x_i \in \Gamma_2} \left\{ \frac{\partial u_1}{\partial x_2}(x_i) \right\}^2$$

$$+ \sum_{x_i \in \Gamma_3} u_2^2(x_i) + \sum_{x_i \in \Gamma_4} u_1^2(x_i) + \sum_{x_i \in \Gamma_4} u_2^2(x_i), \qquad (35)$$

where

$$\boldsymbol{\Phi}_{1i}(\boldsymbol{x}_i) = \frac{\partial \boldsymbol{\tau}_{11}^p}{\partial x_1}(\boldsymbol{x}_i) + \frac{\partial \boldsymbol{\tau}_{21}^p}{\partial x_2}(\boldsymbol{x}_i);\ \boldsymbol{\Phi}_{2i}(\boldsymbol{x}_i) = \frac{\partial \boldsymbol{\tau}_{12}^p}{\partial x_1}(\boldsymbol{x}_i) + \frac{\partial \boldsymbol{\tau}_{22}^p}{\partial x_2}(\boldsymbol{x}_i);\ u_p$$

is the inlet velocity profile given in section (5.2.1).

5.2.3. Results and discussion

The solutions obtained for the velocity field, shear stress and the first normal stress difference are the averages of the last 200 iterations after reaching the steady state. For the Hookean dumbbell model, the parabolic velocity profile is accurately recovered in the downstream region as expected. Figs. 10 and 11 show the polymer shear stress and the first normal stress difference on the middle plane $x_1 = 0.5$ corresponding to the two collocation densities 15x15 and 25×25. The results are in very good agreement with the analytical solution given by eqn. (34). Fig 10 also shows the polymer shear stress and the first normal stress difference at several steps after convergence (steps 120, 121, 122) which depicts small oscillation in steady state solutions as iteration goes on. Such oscillation has its origin in stochastic nature of the microscopic stress calculation, and

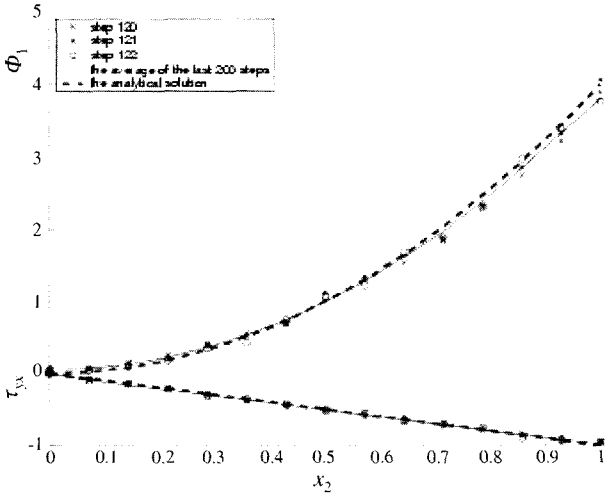

Fig. 10. The steady state planar Poiseuille flow problem using the Hookean dumbbell (Oldroyd-B) model with 15×15 collocation points: the polymer shear stress and the first normal stress difference on the middle plane $x_1 = 0.5$ with respect to x_2 are denoted by 'x' for the step 120, 'o' for step 121, '*' for step 122, solid line for the average of the last 200 steps and dashed line for the analytical solution, respectively.

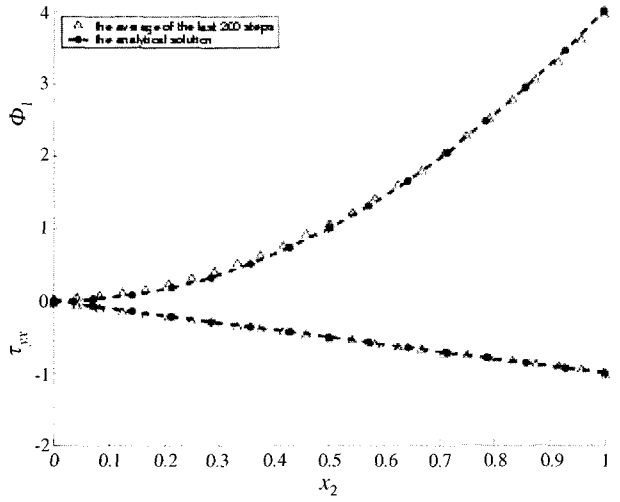

Fig. 11. The steady state planar Poiseuille flow problem using the Hookean dumbbell (Oldroyd-B) model with 25 × 25 collocation points: the polymer shear stress and the first normal stress difference (averaged of the last 300 steps) on the middle plane $x_1 = 0.5$ with respect to x_2 are denoted by 'Δ'. The dashed line represents the analytical solution

therefore the final result is obtained by averaging a large number of these `steady state' solutions.

5.3. Lid driven square cavity

While this problem has attracted the interest of many researchers in the case of viscous fluids, there are very few numerical results for viscoelastic fluids. Mendelson *et al.* (1982) and Grillet *et al.* (1999) use the FEM for the analysis and Tran-Cong *et al.* (2002) employs a BEM and RBF approach for the numerical solution for the Oldroyd-B model. On the other hand, Pakdel *et al.* (1997) performed experiments on an ideal Boger fluid. The results cited above are used here for qualitative comparison with the present results since the fluids used in those studies are different, except for the case of Tran-Cong *et al.* (2002), from the Hookean dumbbell model (Oldroyd-B model) used here. The flow is creeping, isothermal and in a steady state.

The geometry of the computational domain with the chosen coordinate system is shown in Fig. 12a. Let L and H be the width and height of cavity, respectively. Using six different sets of collocation points (11 × 11 + 2); (15 × 15 + 2); (17 × 17 + 2), (19 × 19 + 2), (21 × 21 + 2) and (41 × 41 + 2) whose schematic distribution is described in Fig. 12b, 1000 dumbbells are assigned at each collocation point. The fluid parameters are given by

$$\alpha = \frac{\eta_N}{\eta_o} = 1/9; \quad \lambda_H = 1. \tag{36}$$

Let V be the speed of the lid. The Deborah numbers is given by

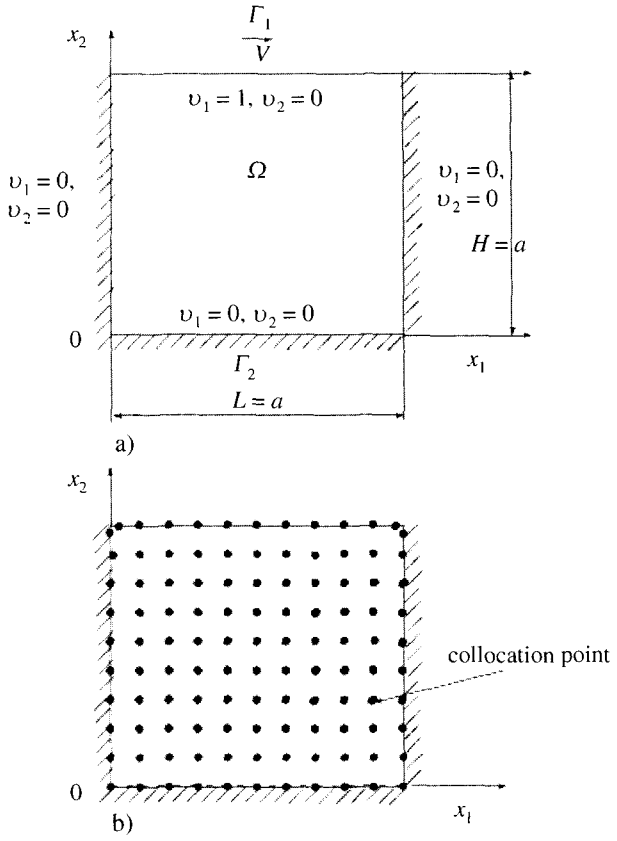

Fig. 12. a) The lid driven square cavity problem: velocity of the upper lid is unity; non-slip boundary conditions apply at the fluid-solid interfaces. b) The collocation point distribution is only schematic.

$$De = \lambda_H \cdot \frac{V}{H},$$

Similar to the works of Tran-Cong *et al.* (2002) and Grillet *et al.* (1999), the Dirichlet boundary conditions are given, in dimensionless form, by (Fig. 12.a):

$$\begin{cases} u_1(\boldsymbol{x}) = 1 & \forall \boldsymbol{x} \in \Gamma_1, \\ u_2(\boldsymbol{x}) = 0 & \forall \boldsymbol{x} \in \Gamma_1, \\ \boldsymbol{u}\ (\boldsymbol{x}) = 0 & \forall \boldsymbol{x} \in \Gamma_2. \end{cases}$$

In order to reduce the number of the degrees of freedom of the problem, the penalty function method for the momentum equation (1) is employed and then the sum square error (20) is rewritten as follows:

$$SSE = \sum_{x_i \in \Omega} \left\{ \alpha \left[\frac{\partial^2 u_1}{\partial x_1^2} + \frac{\partial^2 u_1}{\partial x_2^2} \right]_{x_i} + \frac{P_e}{\eta_o} \left[\frac{\partial^2 u_1}{\partial x_1^2} + \frac{\partial^2 u_1}{\partial x_1 \partial x_2} \right]_{x_i} + \Phi_{1i} \right\}^2$$

$$+ \sum_{x_i \in \Omega} \left\{ \alpha \left[\frac{\partial^2 u_2}{\partial x_1^2} + \frac{\partial^2 u_2}{\partial x_2^2} \right]_{x_i} + \frac{P_e}{\eta_o} \left[\frac{\partial^2 u_2}{\partial x_2^2} + \frac{\partial^2 u_2}{\partial x_1 \partial x_2} \right]_{x_i} + \Phi_{2i} \right\}^2 \tag{37}$$

$$\sum_{x_i \in \Gamma_1} (u_1 - 1)_{x_i}^2 + \sum_{x_i \in \Gamma_1} (u_2)_{x_i}^2 + \sum_{x_i \in \Gamma_2} (u_1)_{x_i}^2 + \sum_{x_i \in \Gamma_2} (u_2)_{x_i}^2$$

where $\Phi_{1i} = \frac{\partial \tau_{11}^p}{\partial x_1}(x_i) + \frac{\partial \tau_{21}^p}{\partial x_2}(x_i)$; $\Phi_{2i} = \frac{\partial \tau_{12}^p}{\partial x_1}(x_i) + \frac{\partial \tau_{22}^p}{\partial x_2}(x_i)$. are known by virtue of the BCF simulation and approximated using TPS-RBFN's and $(.)_{x_i}$ denotes the value of (.) at x_i.

Table 1. The lid driven square cavity flow problem using the Hookean dumbbell model: Trend of the 'mesh convergence' measure, CR defined by with increasing number of collocation points for $De = 1$. N: number of collocation points, *tp*: number of internal test points.

N	*tp*	*CR*
$11 \times 11 + 2$	81	1.0000
$15 \times 15 + 2$	81	0.0447
$17 \times 17 + 2$	169	0.0123
$19 \times 19 + 2$	225	0.0116
$21 \times 21 + 2$	289	0.0097
$41 \times 41 + 2$	443	0.0093

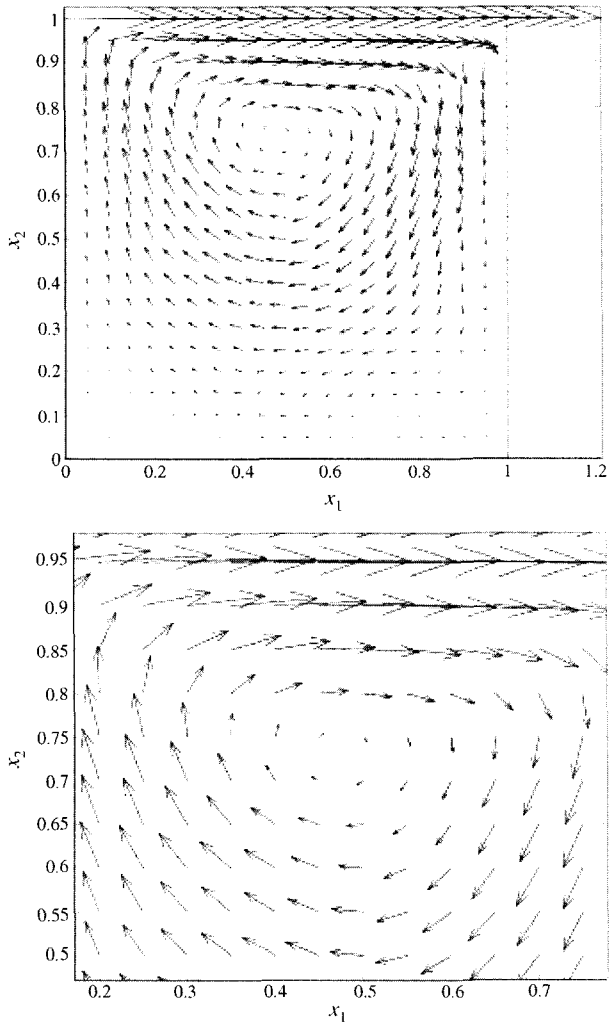

Fig. 13. The lid driven square cavity flow problem using the Hookean dumbbell model: the velocity field (upper figure); the zoomed velocity field around the primary vortex position (lower figure). The parameters are $\alpha = 1/9$, $\lambda_H = 1$ ($De = 1$), $(21 \times 21 + 2)$ collocation points.

5.3.1. Results and discussion

In order to demonstrate that numerical solutions converge to the correct solution, six different sets of collocation points are used as described above and 'mesh convergence' is measured by the following criterion

$$CR = \sqrt{\frac{\sum_{tp} \sum_{i=1}^{2} (u_i^n - u_i^{n-1})^2}{\sum_{tp} \sum_{i=1}^{2} (u_i^n)^2}} \tag{38}$$

where tp is the set of internal test points, u_i^{n-1} is the i^{th} component of the velocity at an internal test point associated

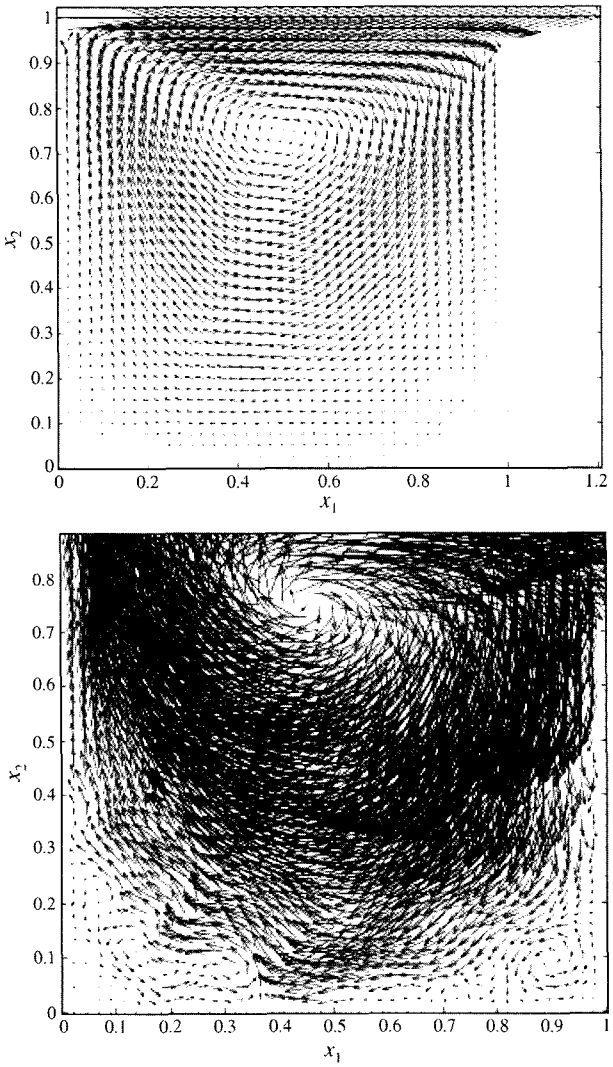

Fig. 14. The lid driven square cavity flow problem using the Hookean dumbbell model: the velocity field (upper figure); the zoomed velocity field around the vortex positions. The parameters are $\alpha = 1/9$, $\lambda_H = 1$ ($De = 1$), $(41 \times 41 + 2)$ collocation points

with the coarser discretisation and u_i^n is the corresponding quantity associated with the finer one. Since the solution (velocity field) is the average of the results of a number of iterations, u_i^{n-1} and u_i^n are the average values at the internal test points. Table 1 reports the trend of CR for the velocity field with increasing collocation density for $De = 1.0$. The process is deemed to have achieved `mesh convergence' when CR is $O(10^{-2})$.

As in the previous examples, the numerical solutions are the average of the results of the last 200 iterations after convergence. In the case of the Hookean dumbbell model, the result is in good agreement with the findings of Tran-Cong *et al.* (2002). Figs. 13 (collocation density $21 \times 21 + 2$) and 14 (collocation density $41 \times 41 + 2$) depict the velocity field for $De = 1$ and Figs. 15 describes the x_1-component velocity profile on the vertical central plane $x_1 = 0.5$ and the x_2-component velocity profile on the horizontal central plane $x_2 = 0.5$. Fig. 16 depicts the velocity field for $De = 1.5$. The results show that the primary vortex center tends to shift upstream and towards the driving lid when De increases. The primary vortex appears to extend up to the walls as shown in Fig. 14 where the size and location of secondary vortices can also be observed in the lower left and right corners. Although the present results can only be compared with Tran-Cong *et al.* (2002) as they used the same model fluid (Oldroyd-B), it is generally in qualitative agreement on the typical flow features reported by Grillet *et al.* (1999), Mendelson *et al.* (1982), and Pakdel *et al.* (1997) in which the vortex shifts upstream as the De number increases. Since the discussion on the efficiency of the control variate variance reduction is not the object of the

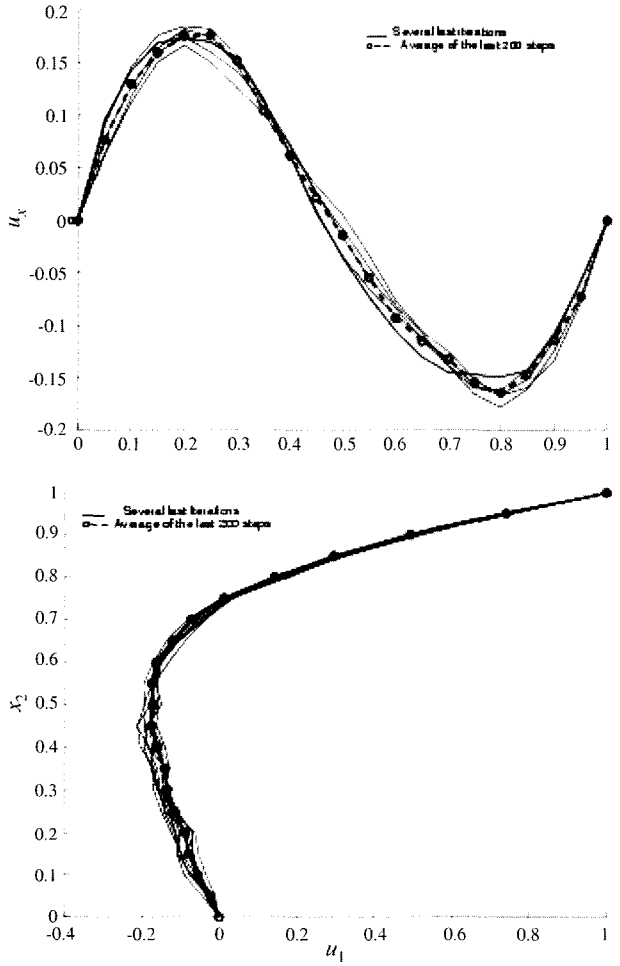

Fig. 15. The lid driven square cavity flow problem using the Hookean dumbbell model: the profile of the velocity component u_2 on the horizontal central plane (upper figure). The profile of the velocity component u_1 on the vertical central plane (lower figure). The solid lines are for the last several steps and '-o-' denotes the average of the results from the last 200 iterations. The parameters are the same as in Fig. 13.

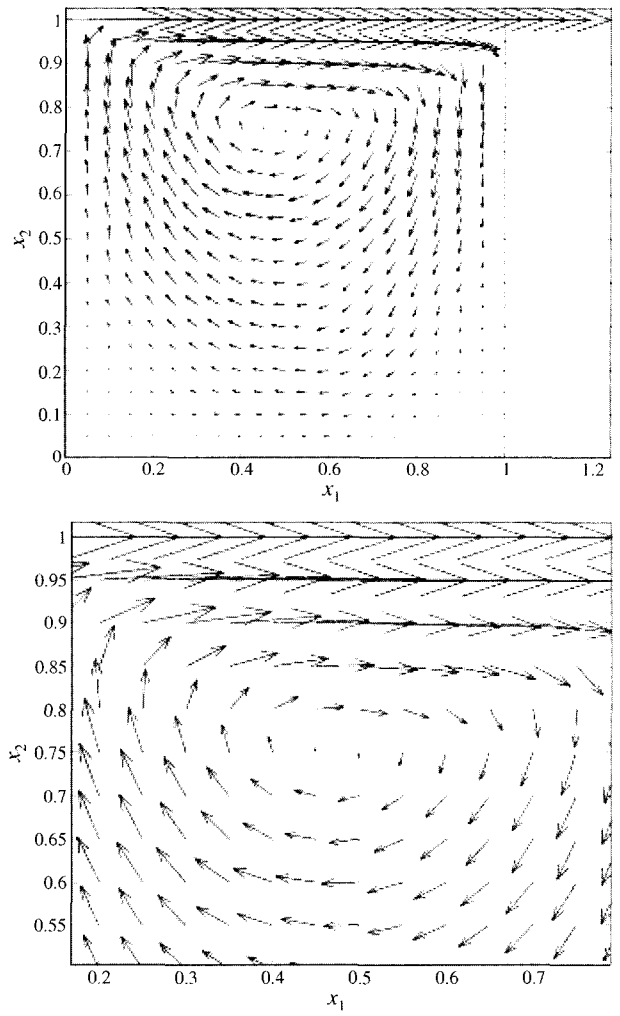

Fig. 16. The lid driven square cavity flow problem using the Hookean dumbbell model: the velocity field (upper figure); the zoomed velocity field around the primary vortex position (lower figure). The parameters are the same as in Fig. 13 except that $\lambda_H = 1.5$ ($De = 1.5$)

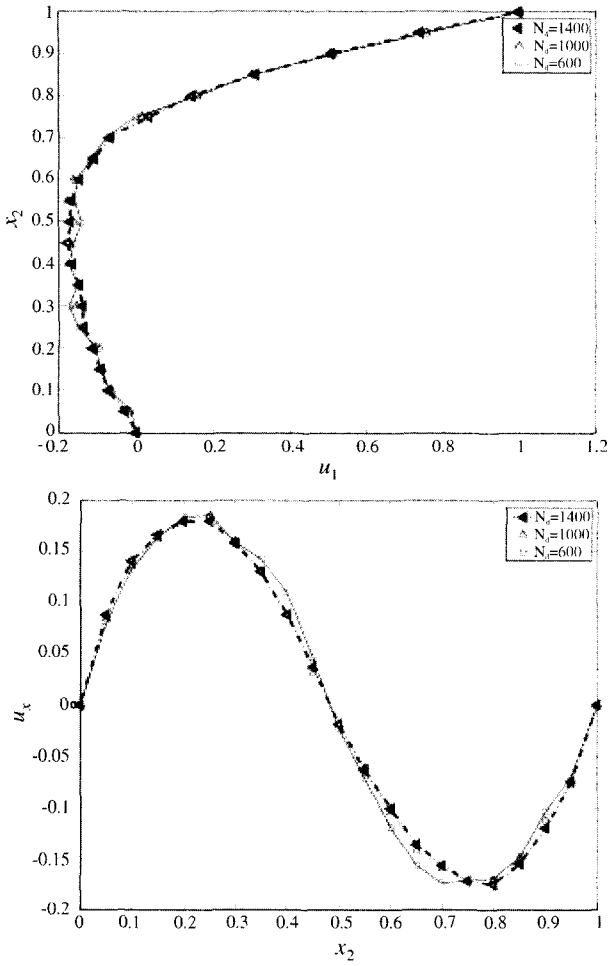

Fig. 17. The lid driven square cavity flow problem using the Hookean dumbbell model: the profile of the velocity component u_2 on the horizontal central plane (lower figure). The profile of the velocity component u_1 on the vertical central plane (upper figure). The average of the results from the last 200 iterations corresponding to the number of dumbbells fixed at each collocation point 600, 1000 and 1400. The parameters are the same as in Fig. 13, $De = 1$.

present work, only an observation of the effect of the number of configuration fields on the velocity fields is given in Fig. 17 for the cases of 600, 1000 and 1400 dumbbells assigned at each collocation point and $De = 1$. The results shown in Fig. 17 demonstrate that the choice of 1000 dumbbells is adequate.

6. Conclusions

This paper reports the development of a computational method for viscoelastic flows using a combination of a RBFN-based element-free method and SST from the Eulerian CONNFFESSIT point of view for 1-D and 2-D problems.

The main advantages of the present method are that: particle tracking is not necessary; variance reduction of the stochastic stress tensor is achieved for the same number of dumbbells used; the noise effect due to the Brownian component is reduced; the method is element-free in both macroscopic and microscopic parts and only an unstructured set of collocation points is required to discretise all governing equations.

The method is verified with standard test problems, namely the start up Couette flow and the planar Poiseuille flow problems. The potential of the method is demonstrated with the successful solution of a non trivial problem, namely the lid-driven square cavity problem.

Acknowledgements

This work is supported by a grant of computing time from the Australia Partnership for Advanced Computing (APAC) National Facility, grant number d72 to T. Tran-Cong. D. Tran-Canh is supported by a USQ Scholarship. This support is gratefully acknowledged. The authors like to thank Prof H.C. Oettinger for his helpful discussions and the referees for their helpful comments.

References

Atluri, S.N. and S. Shen, 2002, The meshless local Petrov-Galerkin (MLPG) method, Tech Science Press, Los-Angeles.

Baker, A.J., 1983, Finite element computational fluid mechanics, McGraw-Hill, New-York.

Belytschko, T., Y. Krongauz, D. Organ, M. Fleming and P. Krysl, 1996, Meshless methods: An overview and recent developments, Comput, Methods Appl. Mech. Engrg. **139**, 3-47.

Bernstein, B., K.A. Feigl and E.T. Olsen, 1993, Steady flows of viscoelastic fluids in axisymmetric abrupt contraction geometry: A comparison of numerical results, *J. Rheol.* **38**(1), 53-71.

Bird, R.B, C.F. Curtiss, R.C. Armstrong and O. Hassager, 1987, Dynamics of polymeric liquids, Vol 2, John Wiley & Sons, New York.

Bonvin, J. and M. Picasso, 1999, Variance reduction methods for CONNFFESSIT-like simulations, *J. Non-Newt. Fluid Mech.* **84**, 191-215.

Cormenzana, J., A. Ledda and M. Laso, 2001, Calculation of free surface flows using CONNFFESSIT, *J. Rheol.* **45**(1), 237-259.

Crochet, M.J., A.R. Davies and K. Walters, 1984, Numerical simulation of non-Newtonian flow, Elsevier, Amsterdam.

Dolbow J., T. Belytschko, 1999. Numerical integration of Galerkin weak form in meshfree methods, Computational Mechanics **23**, 219-230.

Duarte C.A. and J.T. Oden, 1996, An h-p adaptive method using clouds. Comput, *Methods Appl. Mech. Engrg.* **139**, 237-262.

Duchon, J., 1976, Interpolation des fonctions de deux variables suivant le principle de la flexion des plaques minces, RAIRO Analyse Numeriques. **10**, 5-12.

Fedoseyev, A.I, M.J. Friedman and E.J. Kansa, 2002. Improved multiquadric method for elliptic partial differential equations via PDE collocation on the boundary, Compt. and Math.

Applic., **43**(3-5), 491-500.

Feigl, K., M. Laso and H.C. Oettinger, 1995, CONNFFESSIT approach for solving a two-dimensional viscoelastic fluid problem, Macromolecules, **28**, 3261-3274.

Gardiner, C.W, 1990, Handbook of stochastic methods for physics, chemistry and the natural sciences, Springer-Verlag, Berlin.

Golberg, M.A., C.S. Chen and S.R. Karur, 1996, Improved multiquadric approximation for partial differential equations, Eng. Anal. with Boundary Elements **18**, 9-17.

Grillet, A.M., B. Yang, B. Khomami and E.S.G. Shaqfeh, 1999, Modelling of viscoelastic lid driven cavity flow using finite element simulations, *J. Non-Newt. Fluid Mech.* **88**, 99-131.

Haykin, S., 1999, Neural networks: A comprehensive foundation, Prentice Hall, New Jersey.

Hughes, T.J.R., W.K. Liu and A. Brooks, 1979, Finite element analysis of incompressible viscous flows by the penalty function formulation, *J. Comp phys.* **30**, 1-60.

Hulsen, M.A., A.P.G. van Heel and B.H.A.A. van den Brule, 1997, Simulation of viscoelastic flows using Brownian Configuration fields, *J. Non-Newt. Fluid Mech.* **70**, 79-101.

Jendrejack, R.M., M.D. Graham and J.J. de Pablo, 2000, Hydrodynamic interactions in long chain polymer: Application of the Chebyshev polynomial approximation in stochastic simulations, *J. Chem. Phys.* **113**, 2894-2900.

Kansa, E.J., 1990, Multiquadrics-a scattered data approximation scheme with applications to computational fluid dynamics-II: Solutions to parabolic, hyperbolic and elliptic partial differential equations, Computers Math. Applic. **19**(8-9), 147-161.

Kloeden, P.E. and E. Platen, 1995, Numerical solution of stochastic differential equations, Springer, Berlin.

Kloeden, P.E., E. Platen and H. Schurz, 1997, Numerical solution of stochastic differential equations through computer experiments, Springer, Berlin.

Kroger, M., A. Alba-Perez, M. Laso and H.C. Oettinger, 2000, Variance reduced Brownian simulation of a bead-spring chain under steady shear flow considering hydrodynamic interaction effects, *J. Chem. Phys.* **113**, 4767-4773.

Larsson, E. and B. Fornberg, 2001, A numerical study of some radial basis function based solution methods for elliptic PDEs, Tech. Rep. 470, Dept. of Applied Mathematics, Univ. of Colorado at Boulder, CO.

Laso, M. 1998, Calculation of flows with large elongation components: CONNFFESSIT calculation of the flow of a FENE Fluid in a planar 10:1 contraction. In: Adam, M.J., Mashelkar R.A., Pearson J.R.A. and Rennie A.R., Dynamics of complex fluids: Proceedings of the second Royal Society Unilever Indo-UK forum in material science and engineering, Chapter **6**, 73-87, Imperial College Press, London.

Laso, M. and H.C. Oettinger, 1993, Calculation of viscoelastic flow using molecular models: the CONNFFESSIT approach, *J. Non-Newt. Fluid Mech.* **47**, 1-20.

Laso, M., M. Picasso and H.C. Oettinger, 1997, 2-D time-dependent viscoelastic flow calculations using CONNFFESSIT, *AIChE Journal.* **43**(4), 877-892.

Laso, M., M. Picasso and H.C. Oettinger, 1999, Calculation of flows with large elongation components: CONNFFESSIT calculation of the flow of a FENE fluid in a planar 10:1 contraction. In: Nguyen, T.Q. and Kausch, H.H., Flexible polymer chains dynamics in elongational flow: theory and experiment, Chapter **6**, 101-136, Springer, Berlin.

Mai-Duy, N. and T. Tran-Cong, 2001, Numerical solution of Navier-Stokes equations using multiquadric radial basis function networks, Neural Networks. **14**, 185-199.

Melchior, M. and H.C Oettinger, 1996, Variance reduced simulations of polymer dynamics, *J. Chem. Phys.* **105**(8), 3316-3331.

Mendelson, M.A., P.W. Yeh, R.A. Brown and R.C. Armstrong, 1982, Approximation error in finite element calculation of viscoelastic fluid flows, *J. Non-Newt. Fluid Mech.* **32**, 197-224.

Mochimaru Y., 1983, Unsteady-state development of Plane Couette Flow for Viscoelastic Fluids, *J. Non-Newt. Fluid Mech*, **12**, 135-152.

Orr M.J.L., 1999. Recent advances in radial basis function networks. http://www.cns.ed.ac.uk/$\sim$mjo.

Oettinger, H.C., 1996, Stochastic processes in polymeric fluids: tools and examples for developing simulation algorithms, Springer, Berlin.

Oettinger, H.C., B.H.A.A. van den Brule and M.A. Hulsen, 1997, Brownian configuration fields and variance reduced CONNFFESSIT, *J. Non-Newt. Fluid Mech.* **70**, 255-261.

Pakdel, P., S.H. Spiegelberg and G.H. McKinley, 1997, Cavity flows of elastic liquids: Two-dimensional flows, Phys. Fluids **9**(11), 3123-3140.

Phelan, F.R, M.F. Malone and H.H. Winter, 1989, A purely hyperbolic model for unsteady viscoelastic flow, *J. Non-Newt. Fluid Mech.* **32**, 197-224.

Prabhakar, R. and J.R. Prakash, 2002, Viscometric functions for Hookean dumbbells with excluded volume and hydrodynamic interaction, *J. Rheol.* **46**, 1191-1220.

Randles P.W. and L.D. Libersky, 1996, Smoothed particle hydrodynamics: some recent improvements and applications, Comput, *Methods Appl. Mech. Engrg.* **139**, 375-408.

Somasi M. and B. Khomami, 2000, Linear stability and dynamics of viscoelastic flows using time-dependent stochastic simulation techniques, *J. Non-Newt. Fluid Mech.* **93**, 339-362.

Suen J.K.C, Y.L. Joo and R.C. Armstrong, 2002, Molecular orientation effects in viscoelasticity In: J. L. Lumley, S.H. Davis and P. Moin, Annual Review of Fluid Mechanics, **V34** , 417-444.

Tran-Canh, D. and T. Tran-Cong, 2002, BEM-NN Computation of generalized Newtonian flows, Eng. Anal. With Boundary Element 26, 15-28.

Tran-Canh, D. and T. Tran-Cong, 2002, Computation of viscoelastic flow using neural networks and stochastic simulation, *Korea-Australia Rheology Journal* **14**(4), 161-174.

Tran-Canh, D. and T. Tran-Cong, 2003, Meshless computation of 2D viscoelastic flows, *Korea-Australia Rheology Journal*, submitted.

Tran-Cong, T., N. Mai-Duy and N. Phan-Thien, 2002, BEM-RBF approach for visco-elastic flow analysis, Engineering Analysis with Boundary Element, **26**, 757-762.

Travis, B.J., C. Anderson, J. Baumgardner, C.W. Gable, B.H. Hager, R.J. O'connell, P. Olson, A. Raefsky and G. Schubert, 1990, A benchmark comparison of numerical methods for infi-

nite Prandrl number thermal convection in two-dimensional Cartesian geometry, Geophys. Astrophys. Fluid Dynamics, **55**, 137-160.

Zerroukat, M., H. Power and C.S. Chen, 1998, A numerical method for heat transfer problems using collocation and radial basis functions, *Int. J. Numer. Meth. Engng.* **42**, 1263-1278.

Zerroukat, M., K. Djidjeli and A. Charafi, 2000, Explicit and implicit meshless methods for linear advection diffusion-type partial differential equations, *Int. J. Numer. Meth. Engng.* **48**, 19-35.